Palestine Journal of Mathematics

Vol.15(3), (2026) , 532–547 © Palestine Polytechnic University-PPU 2026

Fractal-Fractional SIR Model for Financial Contagion: Mathematical Analysis, Numerical Solutions, and Application

İbrahim Avcı

Communicated by Hijaz Ahmad

MSC 2010 Classifications: Primary 26A33; Secondary 92D30.

Keywords and phrases: Financial contagion, Fractal-Fractional calculus, SIR Model, Mathematical analysis, Adams–Bashforth method.

Abstract Building on the analogy between financial systems and ecosystems, this study extends the classical Susceptible-Infected-Recovered (SIR) model to analyze financial risk contagion among firms. Traditional integer-order models often fail to capture the memory effects, long-range dependencies, and structural complexities found in financial markets and supply chain interactions. To address these limitations, we reformulate the SIR model using the fractal-fractional derivative operator, which accounts simultaneously for fractal geometry and fractional memory effects. The model reflects how past exposures and cumulative financial stress influence both contagion and recovery dynamics, providing a more realistic framework for modeling financial resilience and immunity. We conduct a detailed mathematical analysis to establish the existence and uniqueness of solutions, ensuring the model's well-posedness. Furthermore, we explore the asymptotic stability of both disease-free (risk-free) and endemic (persistent-risk) equilibria. For this purpose, we construct appropriate Lyapunov functionals tailored to the fractal-fractional framework, and derive sufficient conditions for stability, offering deeper insight into systemic risk and resilience thresholds. In addition to theoretical results, we implement a numerical scheme based on the Adams-Bashforth method, adapted to handle the nonlocal nature of fractal-fractional derivatives. This method enables efficient and accurate simulation of the system's dynamic behavior over time. Numerical experiments are conducted using parameter values drawn from selected economic sectors, illustrating the model's capability to capture real-world risk propagation patterns and the delayed effects of interventions. Overall, this study introduces a novel and comprehensive approach to modeling financial contagion, with implications for policymakers, regulators, and financial analysts seeking to understand and mitigate systemic risks in interconnected economic systems.

1 Introduction

Fractional calculus extends differentiation and integration to noninteger orders, with roots that trace back to Leibniz, Liouville, Riemann and others, and a modern theory synthesized in classic monographs (e.g., [1, 2, 3, 4]). Because fractional operators are nonlocal in time or space, they capture memory and heredity effects intrinsic to viscoelasticity, anomalous diffusion, control, and many other complex systems; in epidemiology and networked dynamics, such memory often manifests as long tails and slow relaxation. Among fractional operators, the Caputo and Riemann–Liouville derivatives are widely used for modeling with physically meaningful initial data [5, 6, 7, 8, 9]. More recently, nonsingular-kernel operators (e.g., Atangana–Baleanu) have been proposed to mitigate singularity at the origin while retaining nonlocality [10, 11].

Fractal–fractional (FF) operators combine fractional memory with a fractal (geometric) parameter in one framework, offering an additional degree of freedom to encode multi-scale heterogeneity [12, 13, 14, 15]. Several FF variants coexist (power-law, exponential, Mittag–Leffler kernels; RL/Caputo/ABC senses) and have been analyzed for well-posedness and numerics [16, 17, 18, 19, 20, 21]. Applications now include epidemiology and other complex dynamics where slowly decaying influences and irregular connectivity are salient [22, 23]. At the same

time, open questions remain: (i) principled selection of kernel and operator sense for a given dataset; (ii) identification and interpretation of the memory order and fractal parameter from data; (iii) computational cost and stability for long horizons due to nonlocal memory; and (iv) equivalence/nonequivalence of different FF definitions in inference tasks. These gaps motivate careful model design, transparent assumptions, and cross-checks against classical baselines.

The SIR framework of Kermack and McKendrick and its many extensions underpin the analysis of contagion and diffusion processes [24, 25, 26]. Its appeal is twofold: (i) a clear compartmental interpretation; and (ii) a sharp threshold via the basic reproduction number R_0 that separates die-out from persistence. Mathematically, the baseline (integer-order) system admits standard analysis—existence/uniqueness, positivity and boundedness, equilibria and stability—often via Lyapunov and comparison arguments.

Financial networks exhibit path dependence, clustered exposures, and delayed recovery; shocks rarely decay exponentially. Empirically, long-range dependence and heavy tails are ubiquitous in financial time series and network contagion, suggesting models that remember the past should forecast persistence more realistically. Fractional and FF operators provide exactly this mechanism: the incidence and recovery dynamics inherit memory (fractional order) while the fractal parameter allows coarse encoding of multi-scale connectivity or irregular interaction structure. Prior work has imported epidemic-style models into finance (e.g., liquidity risk and banking distress SIR/SIS variants [27, 28, 29]) and explored fractional tools for financial networks and systemic risk [30, 31, 32]. However, a systematic treatment that (i) formulates a fractal–fractional SIR-type model for financial contagion, (ii) establishes its well-posedness and stability relative to the classical benchmark, and (iii) performs an apples-to-apples numerical comparison under real sectoral data remains limited.

We develop and study a delayed SIR model for financial risk contagion under a fractal—fractional derivative. First, we analyze the baseline (integer-order) delayed system, proving well-posedness (existence/uniqueness, positivity, boundedness), identifying equilibria and the threshold R_0, and establishing stability of the risk-free and endemic states under standard conditions. Second, we upgrade the model by replacing time derivatives with a fractal–fractional operator, and show that while equilibria and the threshold structure are unchanged (being algebraic), the transient dynamics are fundamentally altered. Third, we implement a nonlocal Adams–Bashforth scheme adapted to the FF setting to run controlled numerical experiments: we keep parameters and histories fixed and vary only the memory/fractal orders to isolate memory effects; we also report sensitivity via a response plot (peak I vs. exposure). Finally, using firm-level data from AIDA (Italian automotive sector, 2013–2021), we construct a delay history and calibrate parameters; simulations confirm the $R_0 < 1$ regime under the baseline and quantify how fractional memory stretches time scales. To the best of our knowledge, this combination—FF SIR for financial contagion with rigorous baseline analysis, FF well-posedness/stability discussion, and a data-anchored numerical comparison—fills a gap between theoretical FF calculus and applied financial contagion modeling.

The manuscript is organized as follows. Section 2 recalls the essential background on the fractal–fractional Riemann–Liouville operator with power-law kernel, its integral form, and the tools used later. Section 3 introduces the baseline delayed SIR model for financial contagion and develops its mathematical analysis: well-posedness, equilibria and the threshold $\mathcal{R}_0$, and local stability. Section 4 upgrades the model by replacing classical derivatives with the fractal–fractional operator, explains what changes and what remains, and presents the Adams—Bashforth type numerical scheme with delay. Section 5 details the data and setup. Section 6 reports numerical simulations: baseline vs. fractional-memory dynamics, sensitivity and exposure–memory maps, and robustness checks. Section 7 concludes and outlines directions for future work.

2 Basic concepts

We briefly recall the notions needed for the analysis and numerics. Throughout, $\Gamma(\cdot)$ is the Gamma function, $0 < \alpha < 1$ is the fractional (memory) order, and $0 < \theta \leq 1$ is the fractal (geometric) parameter. For $\theta = 1$ we recover the standard fractional calculus, and for $\alpha \to 1$ we recover classical first derivatives. We adopt the RL power-law operator as a minimal parametric

way to encode long memory and to obtain a clean Volterra integral form compatible with our explicit scheme. For continuous histories, steady-state algebra (and thus $\mathcal{R}_0$) coincides with Caputo. Richer kernels (e.g., Prabhakar) are possible but introduce extra parameters not identifiable with annual data; we leave them to future work.

Definition 2.1. For a function x continuous on $[0,T]$, the fractal derivative of order $\theta \in (0,1]$ is

$$\frac{d}{dt^\theta}x(t) := \lim_{s\to t}\frac{x(s)-x(t)}{s^\theta - t^\theta},$$

whenever the limit exists. For $\theta = 1$ this coincides with the usual derivative.

Definition 2.2. Let x be continuous on $[0,T]$. The fractal–fractional derivative in the Riemann–Liouville sense with power–law kernel is

$$^{\mathbf{FF}}D_{0^+}^{\alpha,\theta}x(t) := \frac{1}{\Gamma(1-\alpha)}\frac{d}{dt^\theta}\int_0^t (t-\xi)^{-\alpha}\,x(\xi)\,d\xi, \qquad 0<\alpha<1,\ 0<\theta\le 1. \tag{2.1}$$

For $\theta = 1$ we recover the classical RL derivative of order α.

Definition 2.3. For $x \in C([0,T])$, the corresponding integral operator is

$$^{\mathbf{FF}}I_{0^+}^{\alpha,\theta}x(t) := \frac{\theta}{\Gamma(\alpha)}\int_0^t \xi^{\theta-1}(t-\xi)^{\alpha-1}x(\xi)\,d\xi. \tag{2.2}$$

Remark 2.4. If $^{\mathbf{FF}}D_{0^+}^{\alpha,\theta}x(t) = f(t,x(t))$ on $[0,T]$, then x satisfies the Volterra equation

$$x(t) = x(0) + {}^{\mathbf{FF}}I_{0^+}^{\alpha,\theta}\big(f(\cdot,x(\cdot))\big)(t) = x(0) + \frac{\theta}{\Gamma(\alpha)}\int_0^t \xi^{\theta-1}(t-\xi)^{\alpha-1}f(\xi,x(\xi))\,d\xi. \tag{2.3}$$

We use (2.3) to pose the initial value problem. For delayed arguments, a continuous history $\phi \in C([-\tau,0])$ supplies $x(\theta) = \phi(\theta)$ for $\theta \in [-\tau,0]$.

Proposition 2.5. *For the linear problem $^{\mathbf{FF}}D_{0^+}^{\alpha,\theta}y(t) = \lambda\,y(t)$ with $y(0) = y_0$, the Volterra form gives*

$$|y(t)| \le |y_0|\,E_\alpha\big(\lambda\,t^\alpha\big), \qquad t \ge 0,$$

where $E_\alpha(z) = \sum_{k=0}^{\infty}\dfrac{z^k}{\Gamma(\alpha k+1)}$ is the Mittag–Leffler function. If $\lambda<0$, then $E_\alpha(\lambda t^\alpha)\to 0$ as $t\to\infty$, giving algebraic-type decay compared to exponentials.

Lemma 2.6. *Let $u \in C([0,T],\mathbb{R}_{\ge 0})$ satisfy*

$$u(t) \le u(0) + \frac{L}{\Gamma(\alpha)}\int_0^t (t-\xi)^{\alpha-1}u(\xi)\,d\xi \quad (0<\alpha<1,\ L\ge 0).$$

Then $u(t) \le u(0)\,E_\alpha\big(L\,t^\alpha\big)$ for $t\in[0,T]$.

3 Baseline model description and analysis

We consider three compartments: $S(t)$ (low–risk/susceptible firms), $I(t)$ (high–risk/contagious firms), and $R(t)$ (recovered/stabilized firms). Parameters are: exposure $a>0$, inflow $b>0$, recovery $\delta>0$, low–risk exit $\gamma_L>0$, high–risk exit $\gamma_H>0$, and a short delay $\tau>0$ capturing scheduled returns from past high risk.

The dynamics are

$$\begin{aligned}
\dot S(t) &= b - \gamma_L S(t) - a\,S(t)I(t) + \delta\,e^{-\gamma_L\tau}\,I(t-\tau),\\
\dot I(t) &= a\,S(t)I(t) - \big(\gamma_H+\delta\big)\,I(t),\\
\dot R(t) &= \delta\,I(t) - \gamma_L R(t) - \delta\,e^{-\gamma_L\tau}\,I(t-\tau),
\end{aligned} \tag{3.1}$$

with continuous, nonnegative histories $(S,I,R) \in C([-\tau,0],\mathbb{R}^3_{\ge 0})$ and $t\ge 0$. We interpret b as a baseline inflow into S, aSI as risk transmission, δI as stabilization into R, and the delayed term $\delta e^{-\gamma_L\tau}I(t-\tau)$ as scheduled return from past high risk that survives low–risk exit during the delay. The delay $\tau=1$ reflects annual reporting/measurement. Moderate deviations of τ primarily shift transient timing (e.g., time-to-peak) without altering equilibria or the threshold $\mathcal{R}_0$ in our calibrated regime.

3.1 Mathematical analysis: baseline delayed SIR

In this section we analyse the baseline delayed SIR system (3.1). Our goal is to ensure the model is mathematically sound and to characterise its qualitative behaviour.

Well-posedness, positivity and boundedness

Theorem 3.1 (Well-posedness). *Given any continuous history* $(S, I, R) : [-\tau, 0] \to \mathbb{R}^3_{\geq 0}$*, system* (3.1) *admits a unique solution* $(S, I, R) \in C([-\tau, T], \mathbb{R}^3)$ *for every* $T > 0$.

Proof. Write $x = (S, I, R)$ and define $F : \mathbb{R}^3 \times \mathbb{R} \to \mathbb{R}^3$ by the right-hand side of (3.1), with $I(t-\tau)$ appearing as a delayed argument. On any bounded set $B \subset \mathbb{R}^3$, F is locally Lipschitz in x because it is polynomial in (S, I, R) and affine in the bounded delayed term $I(t-\tau)$. Standard delay differential equations (DDE) theory (on the phase space $C([-\tau, 0], \mathbb{R}^3)$ with the sup norm) yields local existence, uniqueness, and continuous dependence on the history. Continuous prolongation shows existence on any finite $[0, T]$. □

Lemma 3.2 (Positivity and invariant region). *If* $(S, I, R) \geq 0$ *on* $[-\tau, 0]$*, then* $S(t), I(t), R(t) \geq 0$ *for all* $t \geq 0$*. Moreover, letting* $N(t) := S(t) + I(t) + R(t)$ *and* $\gamma_{\min} = \min\{\gamma_L, \gamma_H\}$*,*

$$\dot{N}(t) = b - \gamma_L (S + R) - \gamma_H I \;\leq\; b - \gamma_{\min} N(t),$$

hence $N(t) \leq \max\{N(0),\, b/\gamma_{\min}\}$ *and the set*

$$\alpha := \{(S, I, R) \in \mathbb{R}^3_{\geq 0} :\; S + I + R \leq M\}, \qquad M := \max\{N(0), b/\gamma_{\min}\},$$

is forward invariant.

Proof. On the boundary $S = 0$ we have $\dot{S} = b + \delta e^{-\gamma_L \tau} I(t-\tau) \geq 0$; on $I = 0$, $\dot{I} = 0$; on $R = 0$, $\dot{R} = \delta I - \delta e^{-\gamma_L \tau} I(t-\tau) \geq -\delta e^{-\gamma_L \tau} I(t-\tau)$, so R cannot jump below zero by continuity (the delayed inflow is bounded). Thus nonnegativity is preserved. Summing the equations gives the inequality for $\dot{N}$; Grönwall implies the bound and forward invariance of α. □

Remark 3.3 (Global existence). Lemma 3.2 bounds $x(t)$ in a compact set; combined with local Lipschitz continuity of the vector field, this rules out finite-time blow-up, so the unique local solution extends to all $t \geq 0$.

Lipschitz and continuous dependence

Lemma 3.4. *Let* $f = (f_S, f_I, f_R)$ *denote the right–hand side of the baseline system* (3.1) *(and the same expressions in the FF model* (4.1)*). On any bounded set* $B \subset \mathbb{R}^3$ *there exists* $L_B > 0$ *such that for all* $x, y \in B$ *and all* $z, w \in B$*,*

$$\big\| f(t, x, z) - f(t, y, w) \big\| \;\leq\; L_B \Big(\|x - y\| + \|z - w\| \Big) \qquad \text{for all } t \geq 0.$$

Proof. Each component is at most bilinear in (S, I, R) and affine in the delayed argument $I(t-\tau)$, so it is locally Lipschitz in (x, z) on bounded sets. The constant L_B follows from polynomial bounds on B (independent of t). □

Theorem 3.5. *Fix* $T > 0$ *and a bounded set of parameters* $(a, b, \delta, \gamma_L, \gamma_H, \tau)$*. Let* x *and* $\tilde{x}$ *be solutions of the same model (baseline or FF) on* $[-\tau, T]$ *with histories* $\phi, \tilde{\phi} \in C([-\tau, 0], \mathbb{R}^3)$ *and the same parameters. Then there exists* $C_T > 0$ *such that*

$$\|x(t) - \tilde{x}(t)\| \leq C_T \|\phi - \tilde{\phi}\|_\infty \qquad (0 \leq t \leq T).$$

Moreover, if the parameters also differ by at most ε*, then* $\|x(t) - \tilde{x}(t)\| \leq C_T \big(\|\phi - \tilde{\phi}\|_\infty + \varepsilon \big)$.

Sketch. For the baseline, subtract the two systems and apply Grönwall to $u(t) = \|x(t) - \tilde{x}(t)\|$ using Lemma 3.4. For the FF case, write the Volterra form and use the fractional Grönwall inequality (Lemma 2.6) with a Lipschitz constant on a bounded absorbing set α. The parameter variation enters additively in the right–hand side, yielding the ε term. □

Equilibria, threshold and stability

Theorem 3.6 (Equilibria and threshold). *Equilibria are obtained by setting the right-hand sides of* (3.1) *to zero (note $I(t-\tau) = I^*$ at equilibrium).*

- *The risk-free equilibrium (DFE) is* $(S^0, I^0, R^0) = \left(\frac{b}{\gamma_L}, 0, 0\right)$.
- *If*

$$\mathcal{R}_0 := \frac{a\,b}{\gamma_L(\gamma_H + \delta)} > 1,$$

then there exists an endemic equilibrium (S^*, I^*, R^*) *with*

$$S^* = \frac{\gamma_H + \delta}{a}, \qquad I^* = \frac{b - \gamma_L S^*}{(\gamma_H + \delta) - \delta e^{-\gamma_L \tau}}, \qquad R^* = \frac{\delta}{\gamma_L}\left(1 - e^{-\gamma_L \tau}\right) I^*,$$

and $I^* > 0$ *if and only if* $\mathcal{R}_0 > 1$.

Proof. Set $\dot{I} = 0$; if $I^* = 0$ then $\dot{S} = 0$ forces $S^0 = b/\gamma_L$ and $\dot{R} = 0$ forces $R^0 = 0$. If $I^* > 0$, then $aS^* - (\gamma_H + \delta) = 0 \Rightarrow S^* = (\gamma_H + \delta)/a$; substituting into $\dot{S} = 0$ gives I^* above (with strictly positive denominator since $(\gamma_H + \delta) > \delta e^{-\gamma_L \tau}$), and $\dot{R} = 0$ yields R^*. The sign condition $I^* > 0$ is equivalent to $b > \gamma_L S^*$, i.e., $\mathcal{R}_0 > 1$. □

Theorem 3.7 (Local stability of the DFE). *At the DFE* $(S^0, 0, 0)$*, the linearization of the I-equation is* $\dot{I} = \big(aS^0 - (\gamma_H + \delta)\big)I$*. Hence the DFE is asymptotically stable iff* $\mathcal{R}_0 < 1$*, and unstable if* $\mathcal{R}_0 > 1$*. Notably, the delay τ does not enter the linearized I-dynamics at the DFE, so the threshold is independent of τ.*

Proof. Direct linearization of the decoupled I-equation yields a scalar ODE with solution $I(t) = I(0)\exp(\lambda t)$, $\lambda = aS^0 - (\gamma_H + \delta)$. Stability is equivalent to $\lambda < 0 \iff \mathcal{R}_0 < 1$. □

Proposition 3.8 (Global attractivity of the DFE). *If* $\mathcal{R}_0 < 1$*, then* $I(t) \to 0$ *as* $t \to \infty$ *and* $(S(t), I(t), R(t)) \to (S^0, 0, 0)$.

On α, $S(t) \le S_{\max}$ for some finite $S_{\max}$. Then $\dot{I} \le \big(aS_{\max} - (\gamma_H + \delta)\big)I$. As trajectories approach the DFE we have $S(t) \downarrow S^0$; a comparison argument with $\dot{y} = (aS^0 - (\gamma_H + \delta) + \varepsilon)y$ and small $\varepsilon > 0$ gives $I(t) \to 0$. Invariance and boundedness then force $(S, R) \to (S^0, 0)$. □

Proposition 3.9 (Endemic equilibrium stability for small delay). *If* $\mathcal{R}_0 > 1$*, the endemic equilibrium is locally asymptotically stable for* $\tau = 0$*; by continuous dependence of the characteristic roots on τ, stability persists for all sufficiently small* $\tau > 0$.

4 Fractal–Fractional SIR Model for Financial Contagion: Mathematical Analysis and Numerical Solutions

We replace each time derivative in (3.1) with the fractal–fractional derivative in the Riemann–Liouville sense with a power-law kernel and fractal rate $\theta \in (0, 1]$ (2.1), thus, the FF SIR model reads

$$\begin{aligned}
{}^{\mathrm{FF}}D_{0^+}^{\alpha,\theta} S(t) &= b - \gamma_L S(t) - a\,S(t)I(t) + \delta\, e^{-\gamma_L \tau}\, I(t-\tau),\\
{}^{\mathrm{FF}}D_{0^+}^{\alpha,\theta} I(t) &= a\,S(t)I(t) - (\gamma_H + \delta)\, I(t),\\
{}^{\mathrm{FF}}D_{0^+}^{\alpha,\theta} R(t) &= \delta\, I(t) - \gamma_L R(t) - \delta\, e^{-\gamma_L \tau}\, I(t-\tau),
\end{aligned} \tag{4.1}$$

with the same nonnegative history on $[-\tau, 0]$ and initial value $x(0)$ induced by the history.

Volterra form and well-posedness

For $n = 1$ in (2.1), the operator is ${}^{\mathrm{FF}}D^{\alpha,\theta} = D_t^{\theta} I^{1-\alpha}$, so (4.1) is equivalent to a Volterra integral system

$$x(t) = x(0) + \frac{1}{\Gamma(\alpha)} \int_0^t (t-\xi)^{\alpha-1} f\big(\xi, x(\xi), x(\xi-\tau)\big)\, d\xi, \tag{4.2}$$

where $x = (S, I, R)$ and f denotes the right-hand sides of (4.1) (the fractal factor reparametrizes time and does not affect local Lipschitz properties).

Theorem 4.1 (Well-posedness). *Assume f in (4.2) is locally Lipschitz in (x, y) uniformly in ξ on bounded sets (which holds here because f is polynomial-affine in its arguments). Then for any continuous nonnegative history on $[-\tau, 0]$ there exists a unique solution $x \in C([-\tau, T], \mathbb{R}^3)$ of (4.1) for every $T > 0$.*

Proof. Fix $T > 0$ and a closed ball $B \subset \mathbb{R}^3$ large enough to contain the history values and the a priori bound below. Define the operator $\mathcal{T}$ on $C([0, T], B)$ by the right-hand side of (4.2), with the history supplying $x(\xi - \tau)$ for $\xi \le \tau$. On $C([0, T], B)$ with the sup norm, using local Lipschitz continuity of f (constant L_B) and the Beta integral,

$$\|\mathcal{T}x - \mathcal{T}y\|_\infty \le \frac{L_B}{\Gamma(\alpha)} \int_0^T (T-\xi)^{\alpha-1} \|x - y\|_\infty \, d\xi = \frac{L_B\, T^\alpha}{\Gamma(\alpha+1)} \|x - y\|_\infty.$$

Choose T small so that the factor is < 1; then $\mathcal{T}$ is a contraction and Banach's fixed point theorem yields a unique solution on $[0, T]$. A standard continuation argument, together with the a priori bound obtained as in Lemma 3.2 (below we prove positivity and boundedness also hold for the FF system), extends the solution to any finite horizon. □

Lemma 4.2 (Positivity and invariant region (FF)). *With nonnegative history on $[-\tau, 0]$, solutions of (4.1) remain nonnegative and bounded for all $t \ge 0$. In particular, there exists $M > 0$ such that $S(t) + I(t) + R(t) \le M$ for all $t \ge 0$.*

Proof. Using (4.2) componentwise with $f_S = b - \gamma_L S - aSI + \delta e^{-\gamma_L \tau} I(t-\tau)$ etc., we see that if S were to attain a negative minimum at some first time $\bar{t} > 0$, the integral representation would contradict minimality because the kernel $(t-\xi)^{\alpha-1}$ is nonnegative and f_S is bounded below by $-\gamma_L S - aSI$ while the nonlocal inflow terms are nonnegative on the boundary. Thus S, I, R cannot cross below 0. Summing the three equations yields ${}^{\mathrm{FF}}D^{\alpha,\theta} N(t) \le b - \gamma_{\min} N(t)$. A fractional Grönwall inequality (applied to $u(t) = N(t)$) gives $N(t) \le N(0)\, E_\alpha(-\gamma_{\min} t^\alpha) + \frac{b}{\gamma_{\min}}\big(1 - E_\alpha(-\gamma_{\min} t^\alpha)\big)$, hence boundedness. □

Equilibria, threshold and stability (FF)

Proposition 4.3 (Equilibria and threshold unchanged). *At equilibrium all FF derivatives vanish, so equilibria solve the algebraic system of the baseline model. Therefore the DFE is $(b/\gamma_L, 0, 0)$ and an endemic equilibrium with $I^* > 0$ exists iff $\mathcal{R}_0 = \dfrac{ab}{\gamma_L(\gamma_H + \delta)} > 1$.*

Theorem 4.4 (DFE stability with memory-driven rates). *Let $\lambda := aS^0 - (\gamma_H + \delta) = (\mathcal{R}_0 - 1)(\gamma_H + \delta)$. The linearized infected equation at the DFE is ${}^{\mathrm{FF}}D^{\alpha,\theta} I(t) = \lambda\, I(t)$. If $\mathcal{R}_0 < 1$ (i.e., $\lambda < 0$) then the DFE is (locally) asymptotically stable and*

$$|I(t)| \;\le\; C\, E_\alpha\big(\lambda\, t^\alpha\big) \quad \text{for } t \ge 0,$$

for some $C > 0$ depending on the initial history. In particular, $I(t) \to 0$ with Mittag–Leffler rate.

Proof. The scalar linear FF equation with RL derivative has solution bounded by a Mittag–Leffler function: writing the Volterra form (4.2) for I, $I(t) = I(0) + \frac{\lambda}{\Gamma(\alpha)} \int_0^t (t-\xi)^{\alpha-1} I(\xi)\, d\xi$. By the fractional Grönwall inequality, $|I(t)| \le |I(0)|\, E_\alpha(\lambda t^\alpha)$. If $\lambda < 0$, $E_\alpha(\lambda t^\alpha) \to 0$ monotonically and the DFE is stable. (When $\theta = 1$ this is classical; the fractal factor reparametrizes time without affecting the sign of λ.) □

In summary of what changes and what does not, replacing the classical time derivatives in (3.1) with the fractal–fractional (RL, power-law) operator leaves the algebraic picture intact—equilibria, feasibility conditions, and the threshold $\mathcal{R}_0$ are unchanged—while it reshapes the transients: exponential relaxations become Mittag–Leffler decays (power-law tails), peaks arrive later and are broader, and integrated burdens such as $\int I(t)\, dt$ and $\int R(t)\, dt$ increase. Thus the FF upgrade preserves analytical transparency but adds realistic, memory-driven inertia that better matches persistent stress observed in data.

4.1 Numerical Adams–Bashforth method

We discretize the fractal–fractional system

$$\begin{aligned} {}^{\mathrm{FF}}D_{0^+}^{\alpha,\theta} S(t) &= b - \gamma_L S(t) - a\, S(t) I(t) + \delta\, e^{-\gamma_L \tau}\, I(t-\tau), \\ {}^{\mathrm{FF}}D_{0^+}^{\alpha,\theta} I(t) &= a\, S(t) I(t) - (\gamma_H + \delta)\, I(t), \\ {}^{\mathrm{FF}}D_{0^+}^{\alpha,\theta} R(t) &= \delta\, I(t) - \gamma_L R(t) - \delta\, e^{-\gamma_L \tau}\, I(t-\tau), \end{aligned} \tag{4.3}$$

in the Riemann–Liouville (power–kernel) sense with order $0 < \alpha < 1$ and fractal parameter $0 < \theta \le 1$. Let a uniform grid $t_n = nh$ ($n = 0, 1, \ldots$), step $h > 0$. Denote the discrete unknowns by

$$S_n \approx S(t_n), \qquad I_n \approx I(t_n), \qquad R_n \approx R(t_n).$$

We write the integral form at t_{n+1}:

$$X(t_{n+1}) = X_0 + \frac{\theta}{\Gamma(\alpha)} \int_0^{t_{n+1}} (t_{n+1} - m)^{\alpha-1}\, H_X(m)\, dm,$$

with $X \in \{S, I, R\}$ and

$$\begin{aligned} H_S(m) &= m^{\theta-1} F_S\big(m, S(m), I(m), R(m)\big), \\ H_I(m) &= m^{\theta-1} F_I\big(m, S(m), I(m), R(m)\big), \\ H_R(m) &= m^{\theta-1} F_R\big(m, S(m), I(m), R(m)\big), \end{aligned}$$

where the right–hand sides are those of (4.3):

$$\begin{aligned} F_S(t, S, I, R) &= b - \gamma_L S - aSI + \delta e^{-\gamma_L \tau} I(t-\tau), \\ F_I(t, S, I, R) &= aSI - (\gamma_H + \delta) I, \\ F_R(t, S, I, R) &= \delta I - \gamma_L R - \delta e^{-\gamma_L \tau} I(t-\tau). \end{aligned}$$

On each subinterval $[t_l, t_{l+1}]$ we approximate $H_X(m)$ by the two–point Lagrange (AB2) interpolant

$$H_{X,l}^*(m) \approx \frac{m - t_{l-1}}{h}\, t_l^{\theta-1} F_X(t_l, S_l, I_l, R_l) - \frac{m - t_l}{h}\, t_{l-1}^{\theta-1} F_X(t_{l-1}, S_{l-1}, I_{l-1}, R_{l-1}),$$

and integrate exactly with the kernel $(t_{n+1} - m)^{\alpha-1}$. As in the template you provided, this yields the weights

$$Y_{(n,l)} = (n+1-l)^\alpha (n - l + 2 + \alpha) - (n-l)^\alpha (n - l + 2 + 2\alpha),$$

$$\widehat{Y}_{(n,l)} = (n+1-l)^{\alpha+1} - (n-l)^\alpha (n - l + 1 + \alpha).$$

For delay evaluation $I(t-\tau)$, let $k(\theta)$ be the index such that $t_{k(\theta)} \le \theta < t_{k(\theta)+1}$. For any time argument $\theta = t_l - \tau$ appearing in (4.3), set

$$I_l^\tau := \begin{cases} I_0(\theta), & \theta < 0 \quad \text{(use given history on } [-\tau, 0]), \\ (1-\lambda)\, I_{k(\theta)} + \lambda\, I_{k(\theta)+1}, \quad \lambda = \dfrac{\theta - t_{k(\theta)}}{h}, & \theta \ge 0 \quad \text{(linear interpolation).} \end{cases}$$

In practice we evaluate I_l^τ wherever F_S, F_R require $I(t_l - \tau)$.

Putting the pieces together, the FF–RL AB2 scheme for (4.3) is

$$S_{n+1} = S_0 + \frac{\theta h^\alpha}{\Gamma(\alpha+2)} \sum_{l=0}^{n} \Big[t_l^{\theta-1} F_S(t_l, S_l, I_l, R_l)\, Y_{(n,l)} - t_{l-1}^{\theta-1} F_S(t_{l-1}, S_{l-1}, I_{l-1}, R_{l-1})\, \widehat{Y}_{(n,l)} \Big], \tag{4.4}$$

$$I_{n+1} = I_0 + \frac{\theta h^\alpha}{\Gamma(\alpha+2)} \sum_{l=0}^{n} \Big[t_l^{\theta-1} F_I(t_l, S_l, I_l, R_l)\, Y_{(n,l)} - t_{l-1}^{\theta-1} F_I(t_{l-1}, S_{l-1}, I_{l-1}, R_{l-1})\, \widehat{Y}_{(n,l)} \Big], \tag{4.5}$$

$$R_{n+1} = R_0 + \frac{\theta h^\alpha}{\Gamma(\alpha+2)} \sum_{l=0}^{n} \Big[t_l^{\theta-1} F_R(t_l, S_l, I_l, R_l)\, Y_{(n,l)} - t_{l-1}^{\theta-1} F_R(t_{l-1}, S_{l-1}, I_{l-1}, R_{l-1})\, \widehat{Y}_{(n,l)} \Big], \tag{4.6}$$

with

$$\begin{aligned} F_S(t_l, S_l, I_l, R_l) &= b - \gamma_L S_l - a S_l I_l + \delta e^{-\gamma_L \tau}\, I_l^\tau, \\ F_I(t_l, S_l, I_l, R_l) &= a S_l I_l - (\gamma_H + \delta) I_l, \\ F_R(t_l, S_l, I_l, R_l) &= \delta I_l - \gamma_L R_l - \delta e^{-\gamma_L \tau}\, I_l^\tau. \end{aligned}$$

For AB2 one needs $l = -1, 0$ values. We set $t_0 = 0$ and obtain (S_0, I_0, R_0) from the history. Compute (S_1, I_1, R_1) with a first–order FF Euler/rectangular rule:

$$X_1 = X_0 + \frac{\theta h^\alpha}{\Gamma(\alpha+1)}\, t_0^{\theta-1} F_X(t_0, S_0, I_0, R_0), \qquad X \in \{S, I, R\},$$

then proceed with (4.4)–(4.6) for $n \ge 1$.

Remarks. (i) The scheme is linear in the history $I_0(\cdot)$ and reuses it whenever $t_l - \tau < 0$. (ii) Complexity is $O(n^2)$ in naive form due to the FF memory; fast convolution can reduce this to $O(n \log n)$ if needed. (iii) For $\alpha \to 1$, $\theta \to 1$, the method reduces to the classical AB2 for the delayed SIR.

5 Data & setup

We use the AIDA–Bureau van Dijk database for Italian enterprises (automotive sector; NACE Rev. 2 codes 2910, 292, 2931, 2932). The observation window is 2013–2021. Let $t = 0$ correspond to 2021 and $t = -8$ to 2013; thus the history window is $[-8, 0]$ (years). Following [33], the working sample contains firms active throughout the window (unbalanced dynamics are reflected in status counts). We normalize by the initial number of active firms N_0 to avoid mixing demographic changes with contagion dynamics. Using time-varying totals would rescale trajectories but would not affect equilibria, thresholds, or comparative statics; we retain N_0 for cross-year comparability.

We adopt a simple, data–driven classification: infected if the firm reported a financial loss in the previous year; recovered if it had loss in the previous year and profit in the current year; otherwise susceptible/low risk. Let N_0 be the number of active firms at $t = 0$; we normalize densities by N_0 so that $S(t) + I(t) + R(t) \le 1$ for all t.

From yearly infected counts $(c_{2013}, \ldots, c_{2021})$ we form

$$I_0(k) = \frac{c_{2013+k}}{N_0}, \qquad k = -8, \ldots, 0,$$

and interpolate by a smooth, shape-preserving curve on $[-8, 0]$ (PCHIP or low-order spline) to obtain a continuous history $I_0(t)$ used by the delayed term $I(t-\tau)$. (We keep the nodal order consistent with $t = 0$ at 2021.)

We calibrate the tuple $(a, b, \delta, \gamma_L, \gamma_H, \tau)$ to match sectoral persistence and scale (see Table 1). The delay τ is set to one year for annual reporting; $\gamma_L, \gamma_H, \delta$ reflect baseline exits and stabilization rates. We do not estimate memory/fractal orders here; they are varied later to isolate memory effects.

The analysis section derived $\mathcal{R}_0 = \dfrac{ab}{\gamma_L(\gamma_H + \delta)}$. For the calibrated values in Table 1 we report the numeric value $\mathcal{R}_0 \approx 0.54 < 1$ and the corresponding critical exposure $a_{\text{crit}} = \dfrac{\gamma_L(\gamma_H + \delta)}{b} \approx 0.51$, which we use as a reference in the response plots.

We use the FF–RL Adams–Bashforth scheme of Section 4.1 with step h chosen to resolve the annual grid (e.g., $h = 0.05$ years). Reliability verified by step refinement: halving h leaves peak I, the area $\int I(t)\,dt$, and the time-to-peak essentially unchanged, and all qualitative conclusions remain intact. We therefore report results at h that balance accuracy and cost. Delayed arguments $I(t-\tau)$ are evaluated from I_0 on $[-8, 0]$ and by linear interpolation for $t > 0$. Unless stated otherwise we keep parameters fixed and vary only the fractional order α (and, optionally, the fractal parameter θ).

Table 1: Calibrated parameters and simulation settings (automotive sector, AIDA 2013–2021). Rates per year; τ in years.

Symbol	Meaning	Value
a	Exposure (transmission) rate	0.2760
b	Inflow to S	0.01061
δ	Stabilization (recovery) rate	0.1527
γ_L	Low–risk exit rate	0.0277
γ_H	High–risk exit (collapse) rate	0.0426
τ	Delay (scheduled return window)	1
N_0	Active firms at $t = 0$ (normalization)	1633

6 Numerical Simulations

We now illustrate the dynamics of the baseline delayed SIR model and its fractal–fractional counterpart using the AIDA automotive dataset described in Section 5. Unless stated otherwise, parameters are fixed at the calibrated values in Table 1, the delay is $\tau = 1$ year, and the history $I_0(t)$ on $[-8, 0]$ is constructed from annual counts. For the FF runs we use the Adams–Bashforth–type scheme of Section 4.1 with step h chosen to resolve the annual grid. We first compare trajectories under integer order ($\omega = \nu = 1$) and fractional memory ($\omega = \nu < 1$), then examine the effect of varying the exposure rate a. Finally, we report sensitivity results and an exposure–memory map (peak I, area $\int I$, and time-to-peak) to quantify how transmission intensity and long-range dependence shape transient risk while leaving the equilibrium and threshold $\mathcal{R}_0$ unchanged.

In the figure 1, the left panel builds the delay history $I_0(t)$ on $[-8, 0]$ from the AIDA counts (2013–2021), normalized by the number of active firms at $t = 0$ ($N_0 = 1633$). Black dots are the annual infected densities c_y/N_0; the dashed curve is a shape-preserving (PCHIP) interpolation that provides a continuous history for the delayed term $I(t-\tau)$. Using this history and the calibrated parameters (Table 1), the right panel shows baseline dynamics of the delayed SIR system: the infected density $I(t)$ declines to zero while the susceptible density $S(t)$ converges to the risk-free level $S^0 = b/\gamma_L$. This behavior is consistent with the threshold value $R_0 < 1$ reported in Section 5: the risk-free equilibrium is asymptotically stable and no endemic state is feasible. The one-year delay τ primarily affects the transient (timing/shape of the early hump) but does not change the long-run outcome; hence the figure provides a baseline against which we later compare the fractional-memory model, where decay is slower due to nonlocal memory.

The figure 2 reports a response curve for the baseline model: for each exposure level a we

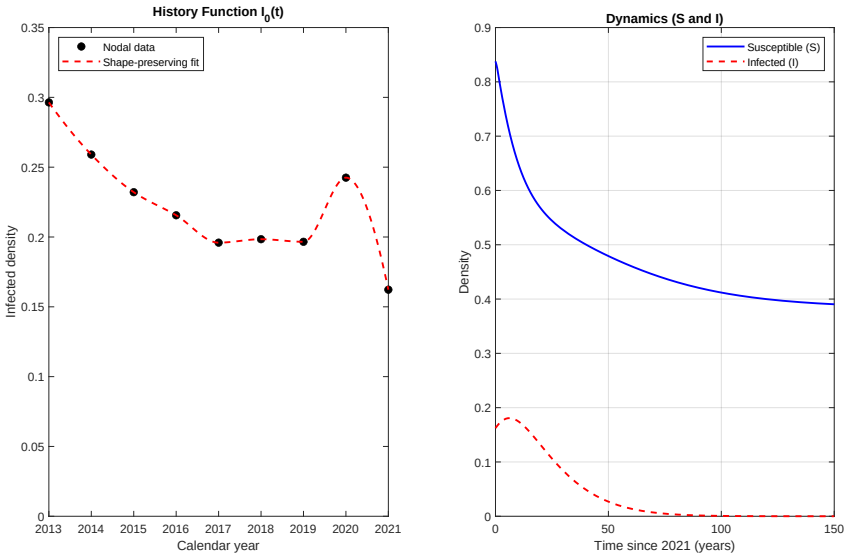


Figure 1: Left: history $I_0(t)$ on $[-8, 0]$. Right: simulated $S(t)$, $I(t)$ up to $t = 150$.

simulate the system and record the peak infected density $\max_{t\geq 0} I(t)$. Blue dots are these simulated peaks; the red dashed vertical line marks the critical value a_{crit} for which $R_0 = 1$ (the threshold reported earlier in Section 5). The upper panel shows the full range $a \in [0.1, 0.6]$; the lower panel zooms near the threshold. The curve increases smoothly with a, indicating that higher exposure produces larger transient stress even when the long–run outcome is risk–free. For $a < a_{\text{crit}}$ (left of the dashed line) trajectories ultimately converge to the disease–free equilibrium (consistent with $R_0 < 1$), but the peak can be nontrivial; for $a > a_{\text{crit}}$ peaks are higher and persistence may occur depending on the delay. The calibrated case (Table 1) lies well to the left of the threshold, which is consistent with the decay of $I(t)$ in our baseline runs. Overall, the figure provides a compact sensitivity summary of how transient risk responds to changes in exposure a and visually corroborates the analytical threshold picture.

In figure 3, we compare the susceptible trajectory $S(t)$ under the same parameters and history, changing only the derivative order of the fractal–fractional RL operator: $\alpha = \theta \in \{1,\ 0.95,\ 0.90\}$. All three curves are monotone and converge to the same limit $S^0 = b/\gamma_L$; hence the equilibrium and the threshold R_0 are unaffected by the memory order. What changes is the transient: smaller α produces visibly slower convergence—the $\alpha = 0.95$ and $\alpha = 0.90$ trajectories lie above the integer case for all displayed times, and at the horizon shown the $\alpha = 0.90$ path remains far from S^0. This illustrates the key role of fractional memory: it reshapes the speed and timing of adjustment without altering the long–run level.

In figure 4, we compare the infected trajectory $I(t)$ under the same calibrated parameters and history, varying only the order of the fractal–fractional RL operator: $\alpha = \theta \in \{1,\ 0.95,\ 0.90\}$. In all cases the threshold reported earlier satisfies $R_0 < 1$, hence $I(t) \to 0$ asymptotically; what changes is the transient. Lower orders produce a later and broader peak—the time of the crest shifts to the right and the crest is slightly higher/flat for $\alpha = 0.90$. After the peak, decay is slower and displays a longer tail for smaller α, consistent with Mittag–Leffler–type relaxation replacing exponential decay. Consequently, the overall burden (e.g., the area $\int I(t)\,dt$ or the half–life) increases as α decreases. This figure thus isolates the role of fractional memory: it reshapes peak timing and persistence without altering the equilibrium/threshold picture.

The figure 5 compares the recovered/stabilized stock $R(t)$ for identical parameters and history while varying only the order of the fractal–fractional RL operator ($\alpha = \theta \in \{1,\ 0.95,\ 0.90\}$).

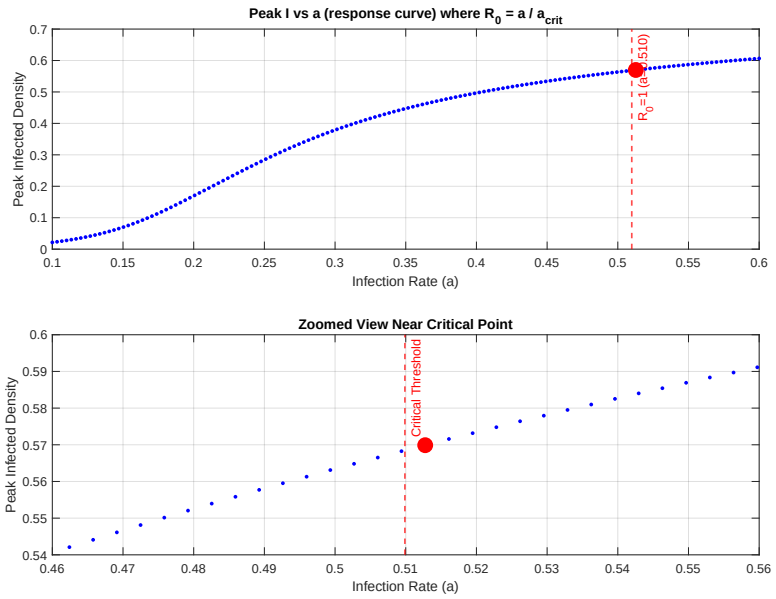


Figure 2: Peak I vs exposure a (response curve).

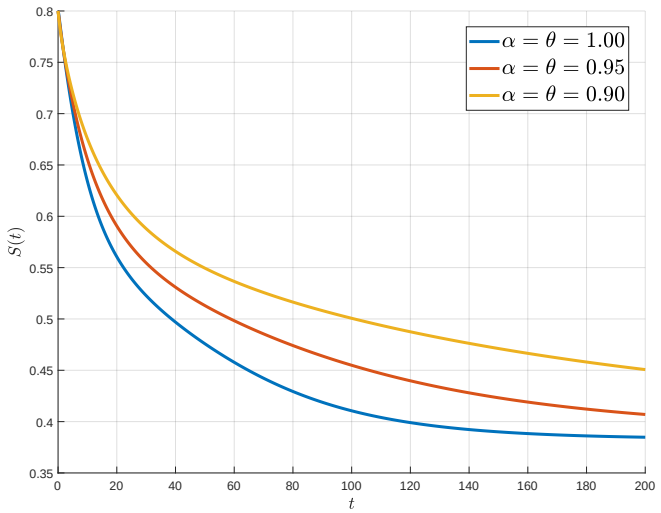


Figure 3: $S(t)$ vs fractional derivative orders.

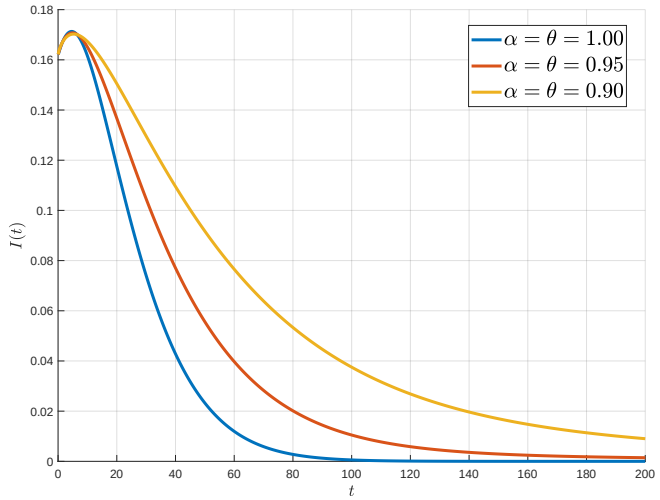


Figure 4: $I(t)$ vs fractional derivative orders.

Lower orders produce systematically slower relaxation: the $\alpha = 0.95$ and $\alpha = 0.90$ curves stay above the integer case at all times, exhibiting heavier tails. The mechanism is twofold: memory slows the decay of $I(t)$, so the inflow $\delta I(t)$ into R persists longer; in addition, fractional relaxation in the R-equation itself delays outflow. Consequently, the overall burden—e.g., the area $\int R(t)\,dt$ or the time needed to fall below a small threshold (such as 1% of the initial value)—increases as α decreases. This mirrors the $I(t)$ behavior and highlights that fractional memory alters persistence and tail behavior without changing the equilibrium/threshold conclusions established earlier.

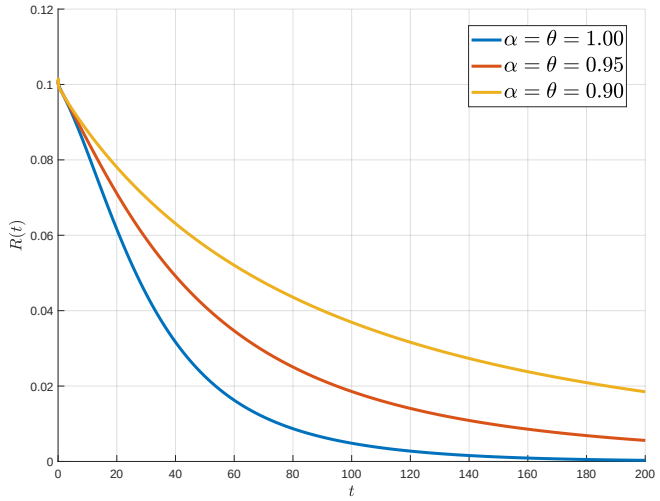
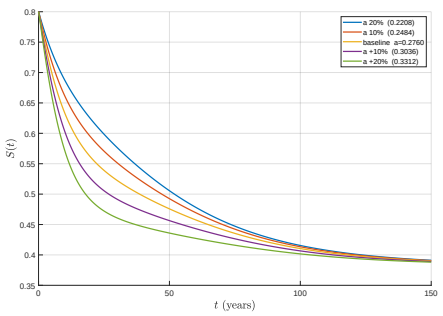


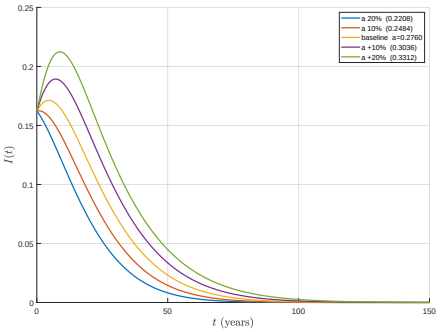
Figure 5: $R(t)$ vs fractional derivative orders.

Figure 6 illustrates a one–at–a–time sensitivity with respect to the exposure rate a by overlaying trajectories for the multipliers $\{0.8, 0.9, 1.0, 1.1, 1.2\}$. Panels (a)–(c) show $S(t)$, $I(t)$, and $R(t)$, respectively. As a increases, the transmission term $a\,SI$ strengthens, so $S(t)$ falls more

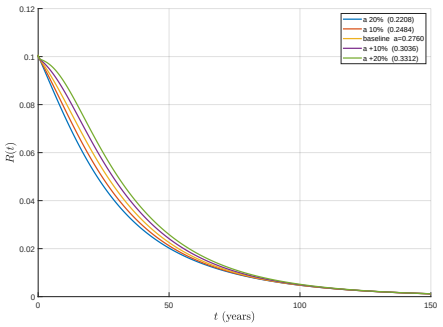
rapidly during the transient (panel (a)), while $I(t)$ exhibits a higher crest and a larger area under the curve (panel (b)); the peak occurs slightly earlier, consistent with faster initial growth. The outflow $\delta I(t)$ into $R(t)$ is therefore larger for longer horizons, yielding a higher $R(t)$ trajectory throughout the transient (panel (c)). In all cases the long–run limits and feasibility conditions are unchanged—$I(t) \to 0$ and $S(t) \to S^0 = b/\gamma_L$—because the reproduction threshold $\mathcal{R}_0 = \frac{ab}{\gamma_L(\gamma_H+\delta)}$ remains below one over the shown range. Thus varying a mainly reshapes the transient burden (peak and duration) without altering the equilibrium picture, quantifying the sensitivity of short–to–medium–run risk to exposure intensity.



(a) $S(t)$ for a multipliers (e.g., 0.8, 0.9, 1.0, 1.1, 1.2).



(b) $I(t)$ for the same a multipliers.



(c) $R(t)$ for the same a multipliers.

Figure 6: Sensitivity to exposure parameter a: trajectories of $S(t)$, $I(t)$, and $R(t)$ under several percentage changes in a.

Figure 7 displays three heat maps over the exposure rate a (horizontal) and the memory order θ (vertical). The dashed vertical line marks a_{crit} where $\mathcal{R}_0 = 1$ (independent of θ). The top panel shows that the peak of $I(t)$ grows mainly with a and, to a lesser extent, with stronger memory (lower θ). The middle panel indicates that the burden $\int I(t)\,dt$ increases with both larger a and lower θ, reflecting heavier fractional tails even when $\mathcal{R}_0 < 1$. The bottom panel reports time–to–peak, which becomes markedly longer as θ decreases (memory delays the crest) and varies non-monotonically with a near the threshold. Overall, a governs outbreak size, while θ governs persistence; the $R_0 = 1$ line separates regimes where responses change most rapidly.

7 Conclusion and future work

We proposed and analysed a delayed SIR–type model for financial risk contagion and its fractal–fractional extension. For the baseline, we established well–posedness (existence, uniqueness, positivity and boundedness), derived the equilibria and the basic threshold $\mathcal{R}_0 = \frac{ab}{\gamma_L(\gamma_H+\delta)}$, and proved local stability of the risk–free state when $\mathcal{R}_0 < 1$. We then replaced classical derivatives with the FF operator and showed that all algebraic features (equilibria, feasibility, and $\mathcal{R}_0$) remain unchanged, while the dynamics change substantially: exponential relaxations are replaced

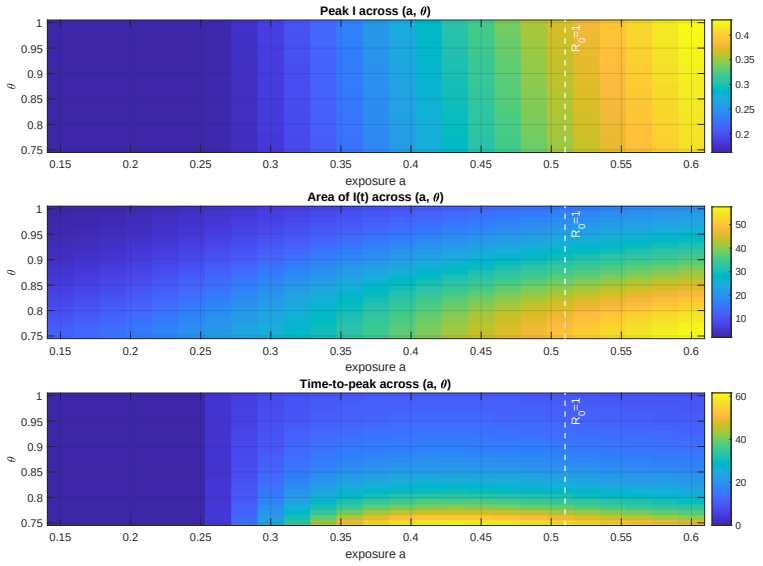


Figure 7: Exposure–memory map for the FF SIR model.

by Mittag–Leffler decays with power–law tails, producing later and broader peaks and slower convergence. An explicit Adams–Bashforth–type scheme was implemented for the FF model. Using annual data from the AIDA database (automotive sector) to construct the history $I_0(t)$ and to calibrate parameters, simulations showed trajectories consistent with theory ($\mathcal{R}_0 < 1 \Rightarrow$ extinction of risk) and highlighted the practical impact of memory: fractional orders slow the dissipation of stress and increase the transient burden. Sensitivity experiments confirmed that exposure a dominates short–run outcomes, while the exposure–memory map revealed a clear interaction between transmission intensity and long–range dependence.

Future work includes jointly estimating the fractal–fractional orders and structural parameters (e.g., likelihood- or Bayesian-based calibration) with uncertainty quantification and kernel comparison (power-law, exponential, Prabhakar); allowing time variation in $a, \delta, \gamma_L, \gamma_H$ and incorporating stochastic or jump shocks to reflect policies and crises; extending to networked, multi-sector or firm-level models with heterogeneous memory to quantify spillovers and resilience; developing control-oriented analyses; strengthening theory and numerics at the critical case $\mathcal{R}_0 = 1$ and with positivity-preserving, convergent schemes for delayed FF systems; and broadening the empirical base by replicating across additional sectors and countries. Together, these steps would turn the framework into a calibrated, decision-oriented tool for monitoring and mitigating systemic financial risk under memory effects.

References

[1] I. Podlubny, *Fractional Differential Equations*, Mathematics in Science and Engineering, Vol. 198, Academic Press, San Diego, 1999.

[2] A. A. Kilbas, H. M. Srivastava, and J. J. Trujillo, *Theory and Applications of Fractional Differential Equations*, North-Holland Mathematics Studies, Vol. 204, Elsevier, Amsterdam, 2006.

[3] K. B. Oldham and J. Spanier, *The Fractional Calculus: Theory and Applications of Differentiation and Integration to Arbitrary Order*, Academic Press, New York, 1974.

[4] F. Mainardi, *Fractional Calculus and Waves in Linear Viscoelasticity*, World Scientific, Singapore, 2010.

[5] M. Caputo, Linear models of dissipation whose Q is almost frequency independent, II, *Geophysical Journal of the Royal Astronomical Society* **13** (1967), 529–539.

[6] Y. Yoda, D. Ouedraogo, I. Ibrango, & M. Barro, Global analysis and numerical simulations of Caputo fractional order derivatives of epidemiological model with coupled incidence. *Palestine Journal of Mathematics*, **14(3)** 2025.

[7] A. Kumawat, and G. Agarwal, Analysis of Infectious Fractional Disease Model. *Palestine Journal of Mathematics*, **15** (2026): 264.

[8] V. K. Regar, H. Singh, and G. S. Sharma, Fractional Hepatitis B Virus Model: An Efficient Approach for Analytical and Numerical Solutions. *Palestine Journal of Mathematics*, **15** (2026): 218.

[9] M. Caputo and F. Mainardi, A new dissipation model based on memory mechanism, *Pure and Applied Geophysics* **91**(1) (1971), 134–147. doi:10.1007/BF00879562.

[10] A. Atangana and D. Baleanu, New fractional derivatives with nonlocal and nonsingular kernel: Theory and application to heat transfer model, *Thermal Science* **20**(2) (2016), 763–769.

[11] M. I. Syam and M. Al-Refai, Fractional differential equations with Atangana–Baleanu fractional derivative: Analysis and applications, *Chaos, Solitons & Fractals: X* **2** (2019), 100013. doi:10.1016/j.csfx.2019.100013.

[12] A. Atangana, Fractal–fractional differentiation and integration: Connecting fractal calculus and fractional calculus to predict complex system, *Chaos, Solitons & Fractals* **102** (2017), 396–406.

[13] A. Atangana and A. Akgül, On solutions of fractal fractional differential equations, *Discrete & Continuous Dynamical Systems – S* **14**(10) (2021), 3441–3457. doi:10.3934/dcdss.2020421.

[14] M. Arif, P. Kumam, W. Kumam, A. Akgul, T. Sutthibutpong *et al.*, Analysis of newly developed fractal–fractional derivative with power law kernel for MHD couple stress fluid in channel embedded in a porous medium, *Scientific Reports* **11** (2021), Article 20858. doi:10.1038/s41598-021-00163-3.

[15] K. Hattaf, A New Class of Generalized Fractal and Fractal–Fractional Derivatives with Non-Singular Kernels, *Fractal and Fractional* **7**(5) (2023), 395. doi:10.3390/fractalfract7050395.

[16] E. M. Omaba, S. E. Mukiawa, and E. R. Nwaeze, On implicit time–fractal–fractional differential equation, *Axioms*, vol. 11, no. 7, 348, 2022. DOI:10.3390/axioms11070348.

[17] E. Addai, L. Garzón, S. Tapaswini, and A. Atangana, A fractal–fractional mathematical model for Zika epidemic with vertical transmission and vector–host interaction, *Physica A: Statistical Mechanics and its Applications*, vol. 601, 127570, 2022. DOI:10.1016/j.physa.2022.127570.

[18] İ. Avcı, H. Lort, & B. E. Tatlıcıoğlu,Numerical investigation and deep learning approach for fractal–fractional order dynamics of Hopfield neural network model, *Chaos, Solitons & Fractals*, 177, 114302, 2023.

[19] N. Almutairi and S. Saber, Application of a time–fractal fractional derivative with a power–law kernel to the Burke–Shaw system based on Newton's interpolation polynomials, *MethodsX*, vol. 12, 102510, 2023. DOI:10.1016/j.mex.2023.102510.

[20] S. Naveen *et al.*, Application of Newton's polynomial interpolation scheme for variable–order fractional derivative with power–law kernel, *Scientific Reports*, vol. 14, 16090, 2024. DOI:10.1038/s41598-024-66494-z.

[21] S. Boulaaras *et al.*, A study on the existence of unique stable approximate solutions: fractal-fractional-based model of an energy supply–demand system, *Boundary Value Problems*, 2025(1), 65, 2025.

[22] E. Okyere, A. Seidu, S. Nantomah, and J. K. K. Asamoah, Fractal–fractional SIRS epidemic model with temporary immunity using Atangana–Baleanu derivative, *Communications in Mathematics and Biostatistics* **10**(4) (2022), 579–609.

[23] S. Sabbar *et al.*, A new computational method for fractal–fractional differential equations with power–law kernel and applications," *Chaos, Solitons & Fractals*, vol. 172, 113434, 2023.

[24] W. O. Kermack and A. G. McKendrick, A contribution to the mathematical theory of epidemics, *Proc. Royal Society A* **115** (1927), 700–721.

[25] H. W. Hethcote, The mathematics of infectious diseases, *SIAM Review* **42**(4) (2000), 599–653.

[26] F. Brauer, Mathematical epidemiology: Past, present, and future, *Infectious Disease Modelling* **2**(2) (2017), 113–127.

[27] O. Mourad *et al.*, "Modeling and mathematical analysis of liquidity risk contagion in the banking system," *Journal of Applied Mathematics*, Article ID 3517342, 2022.

[28] S. Chen and X. Chen, Financial risk contagion and optimal control, *Journal of Industrial & Management Optimization*, vol. 19, no. 4, pp. 2915–2935, 2023. DOI:10.3934/jimo.2022070.

[29] Y. Wei, C. Xie, X. Qing, and Y. Xu, Control of a new financial risk contagion dynamic model based on finite–time disturbance, *Entropy*, vol. 26, no. 12, 999, 2024. DOI:10.3390/e26120999.

[30] M. E. Balcı and N. Özdemir, Fractional calculus: Fundamentals and applications in economics and finance, *Acta Physica Polonica A*, vol. 130, no. 2, pp. 571–575, 2016.

[31] W. Sun, Y. An, and Y. Gao, Systemic risk contagion in China's financial–real estate network: Modeling and forecasting via fractional–order PDEs, *Fractal and Fractional*, vol. 9, no. 9, 557, 2025. DOI:10.3390/fractalfract9090557.

[32] C. D. Constantinescu, J. M. Ramirez, and W. R. Zhu, An application of fractional differential equations to risk theory, *Finance and Stochastics*, vol. 23, no. 4, pp. 1023–1050, 2019. DOI:10.1007/s00780-019-00400-8.

[33] M. Aliano and S. Ragni, A dynamical model with time delay for risk contagion, *Mathematics* **11**(2) (2023), 425.

Author information

İbrahim Avcı, Department of Basic Sciences and Humanities, Faculty of Arts and Sciences, Cyprus International University, Nicosia, Northern Cyprus, via Mersin 10, Türkiye.
E-mail: avcibrahim90@gmail.com, ibrahima@ciu.edu.tr

Received: 2025-10-18
Accepted: 2026-07-10